Heliyon 9 (2023) e20909

Contents lists available at ScienceDirect

Heliyon

journal homepage: www.cell.com/heliyon

Research article

A method of stall recognition using nonlinear feature extraction from the compressor outlet pressure

Marek Mlkvik *, Robert Olšiak, Branislav Knížat

STU in Bratislava, Faculty of Mechanical Engineering, Námestie Slobody 17, Bratislava, 81231, Slovakia

ARTICLE INFO

Keywords:
Centrifugal compressor
Phase-space reconstruction
Attractor
Compressor stall
Non-linear feature extraction
Correlation integral
Correlation dimension
Average mutual information
False nearest neighbour
Stall recognition

ABSTRACT

The paper presents a method for analysing the pressure signal at the compressor outlet, which allows to detect when the machine operating point approaches the area where a stall is about to occur. The signal analysis method is based on nonlinear feature extraction from the dynamic signal. The correlation dimension (d_{corr}) is used to quantify the complexity of the measured signal, its value decreasing if the analysed signal originates from deterministic processes. The results presented indicate that the correlation dimension of the signal decreases at flow rates approximately 10% above the flow rate at which negative effects on machine performance occur. This trend has been observed across multiple rotor speeds. These findings suggest that the perturbations associated with the onset of the stall can propagate to the compressor outlet, leading to less chaotic pressure behaviour that reflects the dynamics of these perturbations. The fact that stall can be identified from the pressure signal in the space between the rotor and the diffuser in its early stages is well known, but the possibility of identifying stall at the compressor outlet, where the perturbations are significantly attenuated, has not been documented in the literature.

List of symbols

a_{ie}	kJ/kg	isentropic work
$C(R_S)$	-	correlation integral
d_{corr}	-	correlation dimension
f_s	Hz	recording frequency
m	-	embedded dimension
Δh	-	entropy difference
N	-	number of elements in the data set
N_{FNN}	-	ratio of false neighbours number to the number of points in reconstructed space
N_i	-	number of points within radius of similarity
p_{in}	kPa	inlet pressure
p_{out}	kPa	outlet pressure
p_b	kPa	barometric pressure

* Corresponding author.
E-mail address: marek.mlkvik@stuba.sk (M. Mlkvik).

https://doi.org/10.1016/j.heliyon.2023.e20909
Received 22 March 2023; Received in revised form 4 October 2023; Accepted 11 October 2023

Available online 17 October 2023

p_{dyn}	kPa	transient pressure at the compressor outlet
Δp_c	kPa	compressor pressure difference
Δp_{nozzle}	kPa	nozzle pressure difference
$\mathbf{p}_k$	-	phase space
p_k	-	element of the phase space $\mathbf{p}_k$
p_i	-	i-th element of p_k
$P\left(p_k, p_{k+t}\right)$	-	joint probability distribution
Q_N	m^3/s	volumetric flow at normal conditions
q	-	dimensionless flow
r	J/kg	specific gas constant
R_i	-	Comparison criterion used in FNN algorithm
R_T	-	Treshold value of R_i used to identify false neighbours
R_S	-	radius of similarity
t	-	index lag
$t_{in}(T_{in})$	°C (K)	inlet temperature
$t_{out}(T_{out})$	°C (K)	outlet temperature
$t_{amb}(T_{amb})$	°C (K)	ambient temperature
Δt_c	°C/(K)	compressor temperature difference
n	rpm	shaft speed
η_{amb}	%	relative humidity of ambient air
y	%	compresibility factor
η_{ie}	%	isentropic efficiency
κ	-	isentropic exponent
τ	s	time delay
σ	kPa	standard deviation from mean

Abbreviations

AMI	Average Mutual Information
CFD	Computational Fluid Dynamics
FNN	False Nearest Neighbour
FFT	Fast Fourier Transform
PIV	Particle image velocimetry
RF	Rotor Frequency

1. Introduction

A centrifugal compressor is a device that finds application in many fields of industry. It plays an indispensable role in the long-distance transport of natural gas, where continuous compensation of energy losses over long pipeline sections is required. This compensation is carried out at compressor stations, which are typically equipped with several compressors and other auxiliary equipment, such as filters or heat exchangers. The operation of compressors at compressor stations is adapted to the customer's requirements, so the machines operate over a wide range of flow rates. The control system of the compressor station must ensure that the compressors' operating point does not fall within the area where a stall or, in the extreme case, a surge occurs. Both phenomena arise due to a reduction in compressor flow. Milder manifestations of stall in the initial stages include a reduction in performance or noise. Both of these manifestations increase in intensity as the flow rate is further reduced and the vibration may increase to such an extent that the compressor is damaged.

As stall or surge is a highly negative phenomenon with potentially dangerous consequences, it has received considerable attention in the scientific literature. Older research papers ([1], [2]) focused mainly on the stall inception, which manifests itself by the formation of disturbances in the space between the impeller and the diffuser. The wavelength of these disturbances varies. Large disturbances are comparable to the circumference of the impeller. Small disturbances typically occupy the space between the few blades of the impeller. According to the wavelength of the disturbances, the terms modal- and spike-type stall inception defined by [3] are used (modal- large wavelengths, spike- small wavelengths). This theme is further developed in [4], [5]. A comprehensive view of the history and progress of research in this field can be found in [6].

Along with research on the physical nature of stall nad surge, considerable attention has been paid to the development of models capable of predicting stall initiation. The first of these models (for axial compressors), based on the hypothesis of propagation of small perturbations, was presented by Emmons [7]. This theory, in various modifications, is still used today ([8]) However, it loses its validity in the case of a fully developed rotating stall, since stall cells can no longer be considered as small perturbations. Slightly more successful have been models based on non-linear perturbation theory [9], [10]. These models provided a deeper understanding of the stall phenomenon, but were not very suitable for its prediction. Today, a widespread approach to predict compressor stall is the use of empirical correlations, which, however, requires a broad experimental data base. In contrast to theoretical models, the application potential of empirical criteria is limited by the range of experimental parameters from which they were derived. Despite the limitations, it is currently a widespread way of stall prediction [11], [12], [13].

In addition to experimental research, numerical simulation (CFD) is now widely used as a tool to provide insight into the processes in the internal spaces of turbomachines. The method allows one to study in detail the occurrence of flow disturbances, their evolution in relation to the geometric parameters of the machine ([14]) or the influence of geometric inaccuracies on the compressor performance ([15]). By applying advanced data processing methods, such as dynamic mode decomposition, detailed studies of disturbance evolution are possible ([16]). Moru ([17]) identified three types of flow structure from near-stall to stable-stall condition in this way. A degree of spatial resolution comparable to CFD is experimentally achievable only with Particle Image Velocimetry (PIV). However, the implementation of this method on a turbo machine is quite challenging, and therefore only a few papers that present the results are found in the literature ([18], [19], [20]).

Recently, research works dedicated to stall detection based on non-linear feature extraction algorithms have started to appear. This approach takes advantage of the fact that no matter how a stall originates, it always has a non-linear nature. This is then reflected in the waveform of the compressor output quantities. The use of chaos theory methods for early stall identification was first proposed by Bright [21]. This followed the work of [22] and [23] in which stall precursors were described in the form of instabilities in the pressure signal. The authors assumed that these precursors were non-linear in nature. Bright used phase space reconstruction to plot the attractors, which he then analysed using the correlation integral. In his results, there was a decrease in the value of the correlation integral as the compressor operating point approached the stall. Importantly, this method detected the onset of stall before it became apparent in the frequency spectrum of the pressure signal. Wang [24] worked with the CFD simulation results. In this work, the authors analysed pressure pulsations at several points located at the outlet of the centrifugal compressor impeller. Based on the fractal dimension of the pressure signal, they were able to identify the stall. This work showed a new direction in stall warning research, which was further developed by Lou [25]. The author used a parameter called approximate entropy to identify small non-linear disturbances in the pressure signal preceding a deep surge. The paper also fairly extensively describes the phase-space reconstruction methodology and the choice of important parameters such as time delay (τ) or embedded dimension (m). Xue [26] then successfully used chaotic bifurcation determinacy to identify stall during compressor velocity transients. These works suggest that algorithms originating in chaos theory have the potential to advance research in the area of early warning of an onset stall.

The motivation of this work is to test the hypothesis that the pre-stall perturbations are detectable in the outlet pressure of the compressor by the non-linear feature extraction method. If this hypothesis is true, then an early stall warning indication could be based on a relatively simple measured pressure signal at the compressor outlet pipe. This method has the potential to be easily implemented in compressors that are currently operating without modifications of such devices. Experimental data were obtained in the framework of a scaled model tests of a compressor designed for use in the transit of natural gas on the territory of the Slovak Republic. The tests were primarily focused on obtaining parameters for setting the anti-surge valve. The secondary objective of the project was to investigate the possibility of early warning of the stall based on continuously measured data when the compressor works. However, the prerequisite was that this stall warning system must operate without interference with the compressor current design. Therefore, it was not possible to take the pressure signal from the impeller or diffuser area. The only option was then to measure the dynamic pressure waveform at the compressor outlet flange. This signal was then analysed in time and frequency domain and also by non-linear feature extraction methods.

However, the use of non-linear feature extraction is quite challenging, as there is no clear methodology for parameter selection in phase-space reconstruction. Therefore, space is given in this paper to explain the entire signal processing methodology from preprocessing to time delay, embedding dimension selection, and correlation dimension computation.

2. Experiment

The machine used in the experiments is a scale model of the first stage of the compressor, located at the compressor station in Veľké Kapušany (Slovakia). To plan the experiment, considerations regarding the model gas and the scale of the model compressor had to be addressed. Atmospheric air was used as the model gas. Discussions were held with the prototype compressor operator on the scaling aspect. To be able to convert the measured results from the model to the prototype, the requirements imposed on the Reynolds number and the Mach number at the tip speed must be met. At the same time, the model must not exceed the power input available in the laboratory. In this respect, a compromise was chosen and the model compressor scale was 1:1.8, resulting in the impeller diameter 600 mm. With this scaling, the power input was sufficiently low for the entire working range of the machine. However, such a down-scale model did not fully meet the criteria to qualify the machine as a compressor. The tip speed Mach number was just below the value of 0.33 required by the similarity theory conditions. Then also the compression ratio p_{out}/p_{in} did not reach the value of 1.1 at maximum speed, which is the fan limit. On this basis, the model was strictly by definition a fan and not a compressor.

For the purpose of the experiments, an open test circuit was built in the STU hydraulic machinery laboratory, which is schematically shown in Figs. 2, 3 and which is depicted in Fig. 1. The circuit was designed according to the requirements of ASME PTC 10-1-1997 [27]. The machine under investigation was driven by a three-phase asynchronous electric motor with speed control by a frequency converter. A 500 mm diameter pipe with a suction manifold was installed in the machine intake. The length of the suction tube was 6000 mm. The measurement point of the variables was at a distance of 800 mm in front of the compressor. At the discharge of the compressor, the pipe diameter was 300 mm. Pressure and temperature measurements were taken 600 mm downstream of the machine outlet. An annubar probe was placed 3000 mm further away as one of the flow measurement methods. Behind the annubar probe, it was necessary to overcome the 2000 mm height difference given by the building arrangement. A throttle valve was placed in the inclined section of the pipe. The end section of the discharge pipe was 6000 mm long (20× inner diameter). A nozzle was

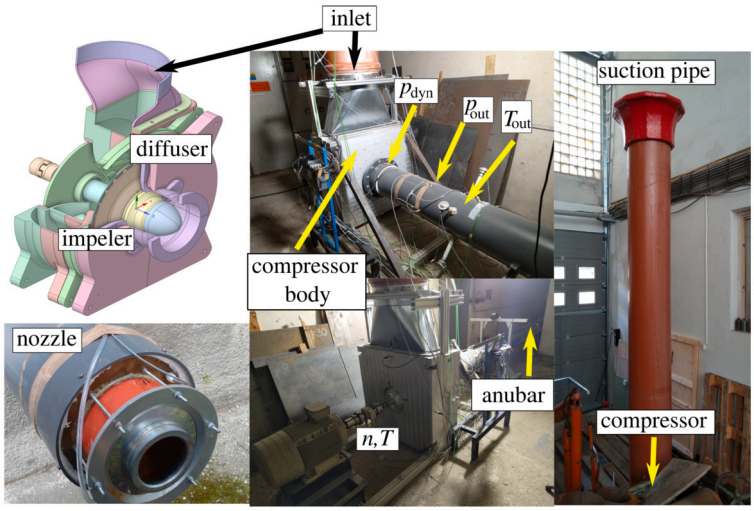

Fig. 1. Real view of test rig.

installed at its end for flow measurement. Before the nozzle, a cell-type flow straightener according to ANSI 210-16 [28] was installed in the pipe. Before the start of the tests, the shape of the velocity profile at the nozzle installation location was verified by pitot tube measurement.

The measurement methods and measurement means were chosen according to ASME PTC 10-1-1997 [27] and [28]. The measurement system installed in the experimental circuit allowed the measurement of both the time-averaged quantities and the dynamic waveform of the compressor outlet pressure. The barometric pressure (p_b) value was measured with an electronic barometer (BD sensors DMP 331). Ambient air temperature t_{amb} and relative humidity η were measured using a coupled sensor (Sensorika HTP-6214). As it was necessary to measure very small differences in static pressures, three measurement methods were implemented to increase the reliability of the results obtained. Two of them for the measurement of time-averaged values and one for the measurement of the time history of the output pressure with a frequency of 25 kHz. The first method for measuring the static pressure difference (Δp_C) was implemented according to international standards [27]. Four MEMS static pressure transducers, rotated 90 degrees, were installed around the perimeter of both the suction and discharge pipelines. The static pressure value was then calculated as the average of the static pressures measured by the four sensors. In the second measurement method, piezometric rings were used according to [28], thus averaging the measured pressure pneumatically. The static pressure values at the inlet and outlet (p_{in}, p_{out}) were also recorded and saved separately. Static temperatures at suction and discharge of the compressor were measured by four sensors located around the perimeter of the piping. From the average values, the temperature difference between suction and discharge (Δt_C) was determined. Volumetric air flow under normal conditions (Q_N) was evaluated from the pressure differential of the orifice (Δp_{nozzle}). Secondary flow measurement was performed using an annubar pneumatic probe (own production).

The experiment started by adjusting the rotor speed with the throttle fully open. While continuously plotting the instantaneous values of the measured quantities, the machine was run in this mode for the time required for all measured quantities to settle, with the slowest settling observed at the outlet gas temperature. In addition to the measured quantities, instantaneous amplitude spectra of the dynamically measured pressure were plotted at 1 sec intervals. After the operating point of the machine was changed, these also exhibited time-varying behaviour: seemingly random appearance and disappearance of peaks throughout the frequency spectrum. The steady state of the peaks in the amplitude spectra was an additional criterion defining the steady state. Once steady state was reached, it was maintained for 15 minutes. If there were no fluctuations in the measured values during this time, the data were recorded. The recorded data were a 12 second average of the instantaneous measured values. The next operating point was set by reducing the flow rate and again repeating the procedure described above to settle the measured parameters. Two separate tests were performed on the compressor in this manner for each of the speeds. At the selected points, a time record of the compressor outlet pressure waveform (p_{dyn}, Fig. 7) was also saved at the same time.

From the measured data, performance curves (Fig. 4(a-c)) were constructed with air flow under normal conditions (Q_N) on the horizontal axis and pressure difference (Δp_c), isentropic work (a_{ie}, eq. (2)) and isentropic efficiency (η_{ie}, eq. (3)) on the vertical axis. The uncertainty analysis was performed according to the recommendations of JCGM 100:2008. The identification of sources of errors, both systematic and random, in the measurement of each variable was performed. For the analysis of the uncertainty of the calculated parameters, it was necessary first to determine the sensitivity of the results to the individual input parameters. The resulting uncertainty was calculated as a combination of individual partial deviations. The expanded uncertainty was obtained by multiplying the combined uncertainty by coverage factor(= 2). Therefore, the error bars that represent the limits of the expanded uncertainty in Fig. 4(a–c) indicate the region into which 95% of the results of repeated measurements would fall at the same operating point.

Stall inception line of the compressor was determined by plotting a curve through the points with a maximum value of a_{ie}. To simplify the comparison of the results, the normalised flow rate (eq. (1)) on the horizontal axis was used, calculated as the ratio of

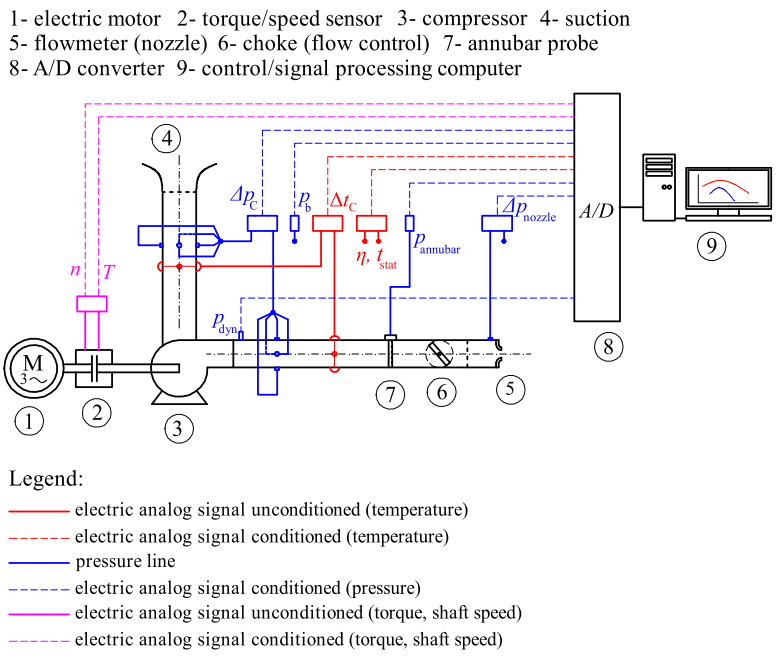

Fig. 2. Schematic drawing of the test rig.

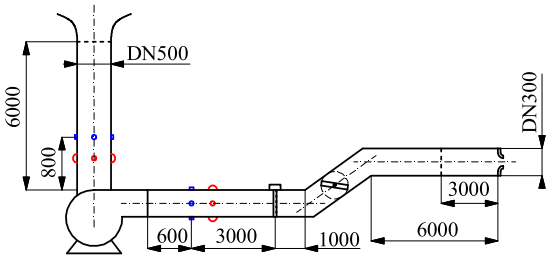

Fig. 3. Main dimensions of the test rig.

the flow rate at the maximum of the curve ($Q(\max(a_{ie}))_{n=\text{const}}$) and the flow rate at a given operating point ($Q_{N,i,_{n=\text{const}}}$). Thus, for $q \leq 1$ the compressor was operating under stall condition.

$$q = \frac{Q(\max\left(a_{ie}\right))_{n=\text{const}}}{Q_{N,i,_{n=\text{const}}}} \tag{1}$$

$$a_{ie} = z_{in} r T_{in} \frac{\kappa}{\kappa - 1}\left[\left(\frac{p_{out}}{p_{in}}\right)^{\frac{\kappa-1}{\kappa}} - 1\right] \tag{2}$$

$$\eta_{ie} = \frac{a_{ie}}{\Delta h} \tag{3}$$

3. Processing of dynamic data

The primary method used in the paper was non-linear feature extraction. However, as [29] points out, the signal obtained by the measurement is burdened with a lot of data that are not related to the problem under analysis. Therefore, the raw signal was subjected to pre-processing before the actual extraction of the stall indicator and its quantification. The first step was to subtract the unnecessary DC component and analyse the amplitude spectra of the AC component of the signal, which helped to determine the frequencies at which the stall was manifested in the analysed data. A low-pass filter was then applied to remove frequencies that were not related to the stall but had a large amplitude and could significantly bias the results of further analyses. These were based on an investigation of attractors obtained by reconstructing the phase space from a one-dimensional data set (compressor output pressure). Reconstruction of the m-dimensional attractor was performed using the time-delay method, which several authors previously used for similar analyses ([25,24,26,30]). The time record of the pressure evolution at the compressor outlet was in the form of a data set

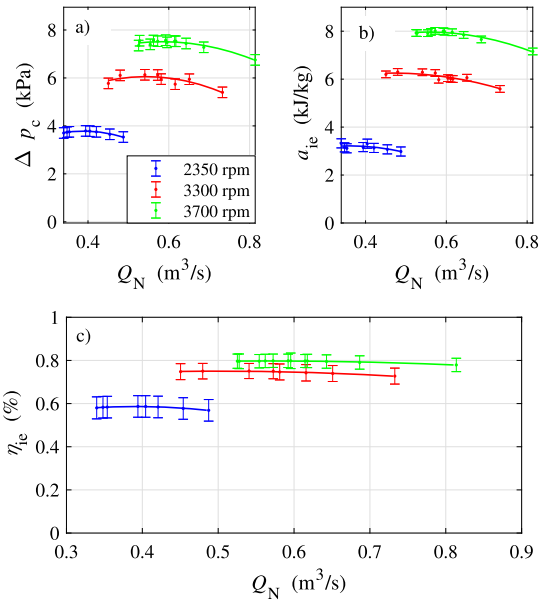

Fig. 4. Performance curves of the compressor: pressure difference (a), isentropic work (b) and isentropic efficiency (c) vs flow of the air at normal conditions. Error bars represent the expanded uncertainity calculated for each measured point.

of points $\{p_i\}$, $i = 1, 2, ..., N$, where N is the number of measured points (record length). This one-dimensional signal was embedded in the space $\mathbf{p_k} \in \mathbf{R}^m$ with dimension m (eq. (4)):

$$\mathbf{p_k} = (p_k, p_{k+t}, p_{k+2t}, \cdots, p_{k+(m-1)t}) \tag{4}$$

For each element of the space $\mathbf{p_k}$ is valid the equation (5):

$$\begin{aligned} p_k &= \{p_i\} \\ p_{k+t} &= \{p_{i+t}\} \\ p_{k+(m-1)t} &= \{p_{i+(m-1)t}\} \\ i &= 1, 2, .., N-(m-1)t \end{aligned} \tag{5}$$

Thus, the phase space consisted of elements that originated from the original time record $\{p_i\}$ such that each additional element was shifted by a value t (index lag) that corresponded to the actual time shift $\tau = \frac{t}{f_s}$. The original one-dimensional signal appeared as an attractor in the reconstructed m-dimensional space, whose analysis was the basis for the identification of the onset stall.

When reconstructing the phase space using the time shift method, the choice of parameters t (or τ) and m is a key factor. The choice of time delay (τ) affects the ability to detect the dynamics of the source signal. When the delay is too small), the resulting attractor is compressed. Conversely, at large time delays, continuity is lost and, hence, information about the dynamics of the signal ([29]). The interdependence between the elements p_k and p_{k+t}, which belong to space $\mathbf{p_k}$, can be expressed by a quantity called average mutual information (AMI, [31]). The term $P\left(p_k, p_{k+t}\right)$ in equations (6) and (7) expresses the joint probability distribution.

$$\mathrm{AMI}(p_k, p_{k+t}) = \sum_{p_k, p_{k+t}} P\left(p_k, p_{k+t}\right) log\left[\frac{P\left(p_k, p_{k+t}\right)}{P\left(p_k\right) P\left(p_{k+t}\right)}\right] \tag{6}$$

As both quantities appearing in the relation (6) come from a single time record $\{p_1\}$, the equation can be simplified to the form (7), where N_p is the length of the time record used. The index lag (t) for the phase space reconstruction is chosen such that the function AMI(t) reaches its first local minimum. The time delay value chosen in this way will ensure that the resulting attractor sufficiently reflects the dynamics of the pressure signal.

$$\mathrm{AMI}(t) = \sum_{i}^{N_p} P\left(\left(\{p_i\}, \{p_{i+t}\}\right)\right) log\left[\frac{P\left(\{p_i\}, \{p_{i+t}\}\right)}{P\left(\{p_i\}\right) P\left(\{p_{i+t}\}\right)}\right] \tag{7}$$

An equally important parameter for the reconstruction of the phase space is the embedded dimension m. The minimum value of m can be determined by the False Nearest Neighbour (FNN) algorithm proposed in 1992 by Kennel [32]. It is an iterative procedure that allows us to identify points on the reconstructed attractor that have become neighbours as a result of the projection of the original attractor into a space with a lower dimension. Therefore, these are called false neighbours. The algorithm works on the principle

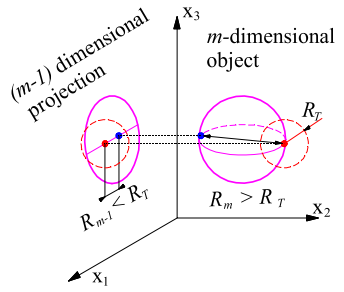

Fig. 5. Generation of false neighbours by embedding the atractor into less dimensional fractal space.

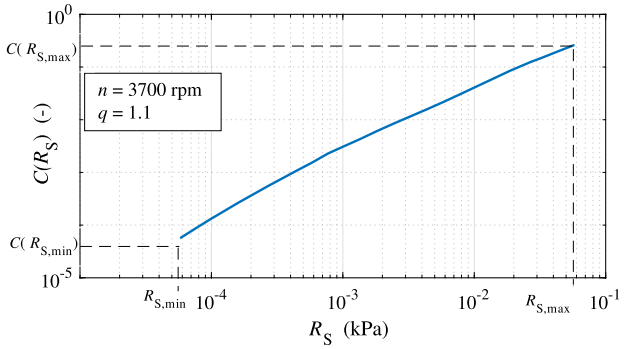

Fig. 6. Example of the correlation integral. $R_{S,\,max} = 0.2\sigma$, $R_{S,min} = 0.2 \times 10^{-3}\sigma$.

of determining the distance between a point p_i from the time record and its nearest neighbour p_i^* from m-dimensional space. The distance between these points can be expressed as $\| p_i - p_i^* \|$. Identification of the false neighbour is done based on the relation (8). Thus, a characteristic of false neighbours is that they move away to a distance, where criterion R_i (eq. (8)) exceeds the threshold value R_T when embedded in a higher-dimensional space (Fig. 5).

$$R_i = \frac{| p_{i+1} - p_{i+1}^* |}{\| p_i - p_i^* \|} > R_T \tag{8}$$

As m increases, the ratio of false neighbours to the number of points in the reconstructed space (N_{FNN}) gradually decreases. The minimum value of m is found when the condition $N_{FNN} \leq N_{FNN,\,max}$ is satisfied, where $N_{FNN,\,max}$ is the chosen criterion.

Reconstruction of the phase space produces an m-dimensional object (attractor) whose analysis can provide information about the dynamics of the source signal. Stall is a phenomenon, accompanied by disturbances in the pressure field, that introduces components into the pressure time history that are deterministic in nature and can be distinguished from ordinary noise. The correlation dimension (d_{corr}) was used as a parameter capable of detecting the effect of stall on the output pressure. It reflects the degree of chaotic behaviour of the signal, while, in general, a chaotic signal has a higher correlation dimension than a signal that is the result of processes governed by certain laws. To calculate it, it is first necessary to determine the number of points located around an i-th point on the attractor within a distance $N_i(R_S)$ (R_S denotes the radius of similarity). The correlation integral $C(R_S)$ (eq. (9)) is then calculated for the range $R_S \in [R_{S,min}; R_{S,max}]$. The correlation dimension then represents the slope of the linear fit curve $C(R_S)$ within this interval (Fig. 6). The parameters $R_{S,\,min}$ and $R_{S,\,max}$ were defined in this document as $0.2 \times 10^{-3}\sigma$ and 0.2σ, where σ is the standard deviation of the analysed data set from the mean. The values were chosen so that for all the signals we analysed, the $C(R_S)$ curves are easily linearly approximated.

$$C(R_S) = \frac{2}{N(N-1)} \sum_{i=1}^{N} N_i(R_S) \tag{9}$$

4. Results

Fig. 7 shows the AC component of the static pressure p_{dyn} measured in the time domain for different flow rates. The qualitative character of the signal did not change much when moving from the far-stall region to the near-stall region. The signal contained relatively high pulsation amplitudes, but these were due to the location of the pressure sampling just downstream of the compressor body. A slight change in the nature of the signal was observed when the flow rate dropped to $q < 1$, a regime where the effects of stall on the compressor power curves were already observable, and its acoustic manifestations were evident. In Fig. 7, oscillations with a period of approximately 20 rotor revolutions are visible. However, typical stall manifestations in the form of pressure spikes were

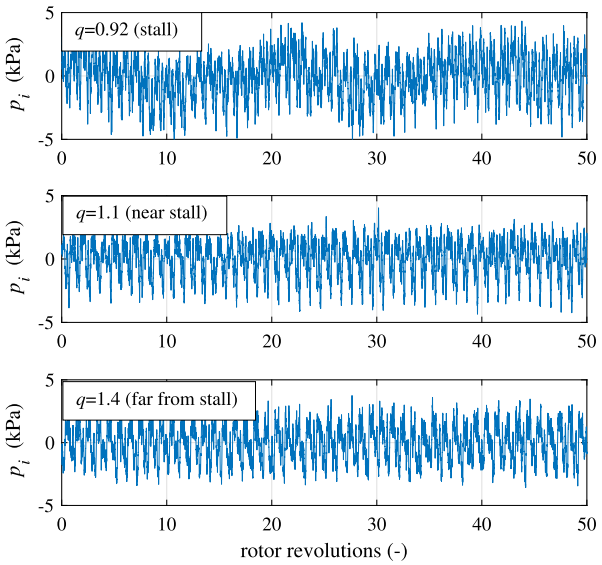

Fig. 7. Example of the measured pressure signal p_{dyn} (only AC component). The relative zeros are the DC components of the individual signals. Each panel of the image represents the signal for different flow of the gas (q) at stall, near stall and far from stall conditions.

not observed. This is a difference from the work in which pressure measurements were performed in the compressor body ([25,26]). The observed oscillations do not necessarily originate from stall-induced perturbations. An unambiguous link of observed qualitative changes in pressure waveform with stall-induced perturbations would require correlation with pressure measurements in the space between the rotor and the diffuser.

As the effect of stall on the output pressure signal was not demonstrable in the time domain, the data were converted to the frequency domain using a discrete Fast Fourier Transform. The results are shown in Figs. 8-10. In this section, only frequencies in the range from 0 to 100 Hz will be analysed, as the effects of stall on the compressor output pressure have been observed in this range.

The effect of decreasing airflow on the output pressure signal was best seen at the highest shaft speed (Fig. 8). When the operating point was in a region where stall was not expected to occur ($q > 1$), a single peak was present in the displayed portion of the spectrum, corresponding to the rotor frequency (RF = 61.6 Hz). The signal in the remaining part of the spectrum corresponded to noise. When the flow rate was reduced to values where the power curves were negatively affected ($q \leq 1$), a signal appeared in the low frequency region (< 15 Hz) whose peak amplitudes reached approximately 20% of the amplitude of RF. Along with this signal, the stall began to manifest itself acoustically. Similar results were obtained at a shaft speed of 3300 rpm (RF = 55 Hz, Fig. 9). Except for the rotor frequency, there was only noise in the amplitude spectrum in the range from 0 to 100 Hz until the q value dropped below 1, at which point the signal appeared at low frequencies. In this case, the maximum amplitudes of this signal reached approximately 25% of the amplitude of rotor frequency. When the compressor was tested with the lowest shaft speed (2350 rpm), the low-frequency signal accompanying the decrease in compressor performance no longer appeared as soon as $q = 1$ was exceeded, but only at $q \leq 0.86$. Moreover, here this signal was weaker compared to the previous cases, as the amplitudes were about 10% of the rotor frequency amplitudes. However, in this regime, the machine was operating at the lower limit of its capabilities with very little pressure increment. Therefore, it can be assumed that the pressure pulsations arising from the disturbances of the flow field caused by the onset stall were milder and may have been attenuated between the point of origin and the point of pressure sampling, thus becoming untraceable for FFT analysis as they were indistinguishable from noise.

Changes in the amplitude spectrum due to changes in compressor flow indicate that perturbations caused by stall did manifest with measurable intensity in the outlet pipe. Therefore, with FFT analysis, it was possible to detect stall as long as the compressor worked in modes where $q \leq 1$ and stall also began to manifest itself in increased noise and vibrations. However, given the negative effects of vibrations on the mechanical parts of the compressor, it would be preferable to predict the stall before these effects are observable. Therefore, the signal was analysed in detail using methods arising from chaos theory.

4.1. Phase-space reconstruction of the pressure signal

The first step of further analysis was to reconstruct the attractors from the one-dimensional data series. Attractors for different operating points of the compressor at 3700 rpm are plotted in Fig. 11, whose amplitude spectra are shown in Fig. 8. An AC signal component of length corresponding to 50 impeller revolutions was used to create these attractors. All the depicted patterns are similar to each other and the presence of stall cannot be noticed from their shape. However, as shown in Fig. 8, the presence of stall is only evident at frequencies below 15 Hz. Furthermore, this part of the signal had a small amplitude. Therefore, all frequencies higher than 15 Hz acted as noise when the attractor was formed. Therefore, a low-pass filter was used to remove the unnecessary part of the signal.

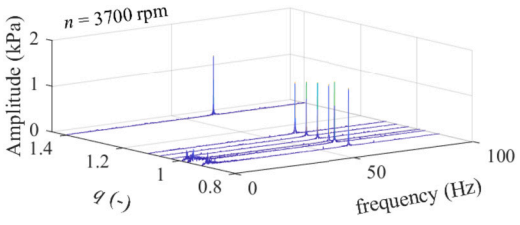

Fig. 8. Amplitudes spectra for n = 3700 rpm).

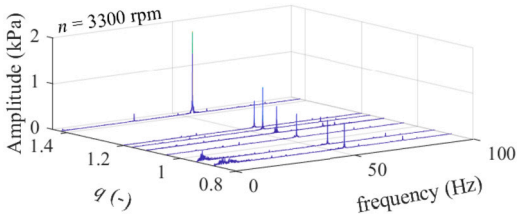

Fig. 9. Amplitudes spectra for n = 3300 rpm).

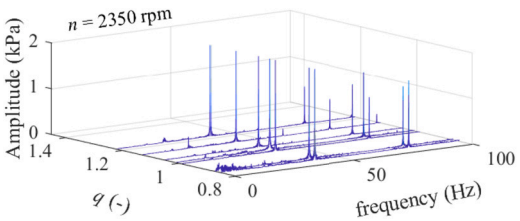

Fig. 10. Amplitudes spectra for n = 2350 rpm).

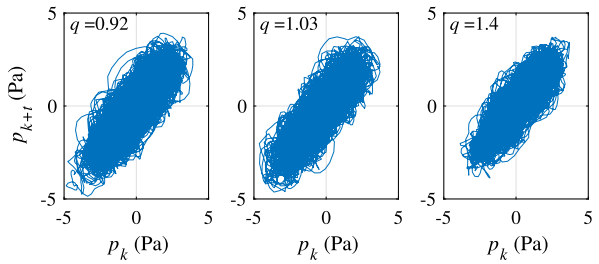

Fig. 11. Atractors obtained from the unfiltered pressure signal at $n = 3700$ rpm. Each panel of the image represents the signal for different flow of the gas at stall ($q = 0.92$), near stall ($q = 1.03$) and far from stall ($q = 1.4$) conditions, $m = 3$, $t = 10$.

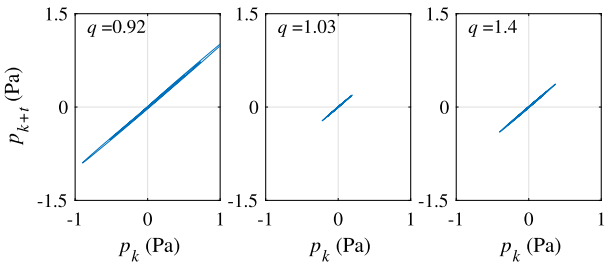

Fig. 12. Atractors obtained from the low-pass filtered pressure signals at $n = 3700$ rpm. Each panel of the image represents the signal for different flow of the gas at stall ($q = 0.92$), near stall ($q = 1.03$) and far from stall ($q = 1.4$) conditions, $m = 3$, $t = 10$.

The attractors that were reconstructed from the filtered signal are depicted in Fig. 12. These attractors already showed a change when the compressor flow was reduced. Similarly to the amplitude spectra, the change appeared only at $q < 1$, so qualitative changes in the shape of the attractors did not produce new information compared to the FFT analysis. However, the need for filtering the measured data before starting the phase-space reconstruction and its quantitative analysis became apparent.

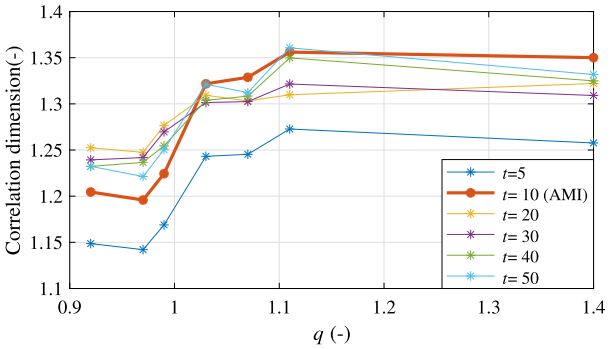

Fig. 13. Comparison of the correlation dimension for different time delays of the reconstructed fractal spaces, $n = 3700$ rpm, $m = 3$.

Although signal filtering proved to be an essential step in signal pre-processing, other aspects had to be addressed in the phase-space reconstruction. To convert the one-dimensional time record of the compressor output pressure (p_{dyn}, Fig. 2) into a multidimensional one, the correct time delay (τ) or the lag index (t) for the discrete data and the embedded dimension of the reconstructed phase space (m) had to be determined. Both of these parameters affect the correlation dimension of the reconstructed attractor, which will be used further to quantify the complexity of the signal and identify perturbations in the measured signal.

The relationship between the correlation dimension and the dimensionless flow parameter q is shown in Fig. 13 to 15. All presented curves clearly show that the correlation dimension decreased if the compressor operating point moved toward stall ($q \leq 1$). This suggests that the small disturbances associated with the onset of stall changed the dynamics of the measured signal, which became less stochastic.

Data sets that are the result of deterministic phenomena generally have a lower value of the correlation dimension than those that are the result of stochastic phenomena. The reason can be explained using the simplified example of an attractor in the form of a line segment embedded in a 2D space that is the result of deterministic processes. Stochastically generated points in 2D space will form an attractor in the shape of a cluster of points. If the radius of the neighbourhood of an arbitrary points on a given attractors increases, the number of points inside that neighbourhood will grow more slowly in the case of a line-shaped attractor. The correlation dimension of the ordered set of points will be smaller compared to the randomly generated set because it inherently expresses the rate of increase in the number of neighbours as a function of the size of the selected neighbourhood.

The curves in Fig. 13, 14 show that the value of the correlation dimension was significantly affected by the choice of the parameters m and t. The influence of these parameters, which are crucial in the reconstruction of the phase space, is therefore analyzed in detail below.

When reconstructing the phase space, the AMI algorithm was used for the initial estimate of the index lag (t). Subsequently, the correlation dimension was evaluated as a function of flow. The same procedure was repeated for values between 0.5 and 5 of the original index lag. The obtained dependencies of the correlation dimension on q are shown in Fig. 13. Although the shape of all the depicted curves is comparable, at $t = 10$, obtained using the AMI algorithm, the difference between the maximum (≈ 1.35) and the minimum (≈ 1.2) is the largest. As the index lag increased, there was a gradual decrease in the difference in the correlation dimension for the high- and low-flow regimes. This suggests that as the index lag increased, information on signal dynamics was being lost. This is unfavourable for stall detection, since it is the relative change in the value of the correlation dimension that serves as a comparison criterion.

For the estimation of the embedding dimension (m) of the reconstructed phase space, the FNN algorithm was followed as the first step. In Fig. 14 it can be seen that increasing the value of this parameter from the initial value of $m = 3$ to a value of 80 led to the shifting of the curves in both directions (up and down). However, the relative change in the correlation dimension as the flow rate decreased, which was more pronounced in the range $m = 3$ to 10 in the presented data, is more relevant for the indication of an incoming stall. Therefore, the FNN algorithm was followed to determine m in subsequent analyses.

It can be concluded that an incorrect choice of the time lag and the embedded dimension can reduce the sensitivity of the presented method for stall identification. Therefore, it is recommended to choose these properties based on algorithms that derive values from the parameters of the analysed signal. This ensures that the data evaluation methodology is unified regardless of the machine operating point. Therefore, when evaluating and analysing signals obtained at different compressor speeds, the choice of τ and m was based on the AMI and FNN algorithms when reconstructing the phase space.

The qualitative dependence of the correlation dimension on the dimensionless flow rate did not change when the compressor speed was varied (Fig. 15). As the compressor operating point moved toward stall, the value of the correlation dimension began to decrease for all shaft speeds tested. This qualitative change was clearly observable before the effects of the incoming stall began to manifest itself by noise and vibrations at $q \leq 1$. The observed dependence can be explained by the fact that small perturbations prior to stall inception induced pressure fluctuations at frequencies less than 15 Hz. Since these fluctuations were deterministic, the complexity of the signal was reduced compared to the higher flow rates. The pressure measurements were made on the discharge line, so the effect of stall on the amplitude of the pressure fluctuations was low and thus did not manifest itself in the amplitude spectra soon enough to indicate the stall inception.

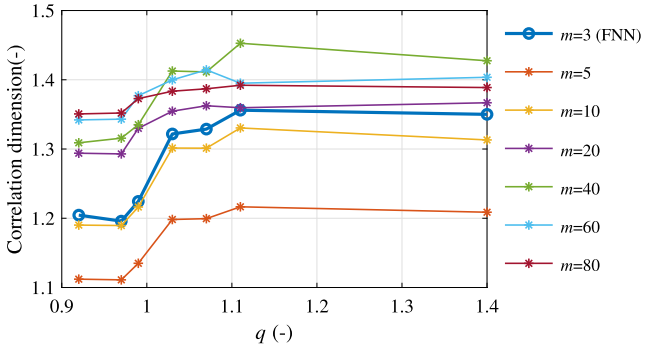

Fig. 14. Comparison of the correlation dimension for different embedding dimensions of the reconstructed fractal space, $n = 3700$ rpm).

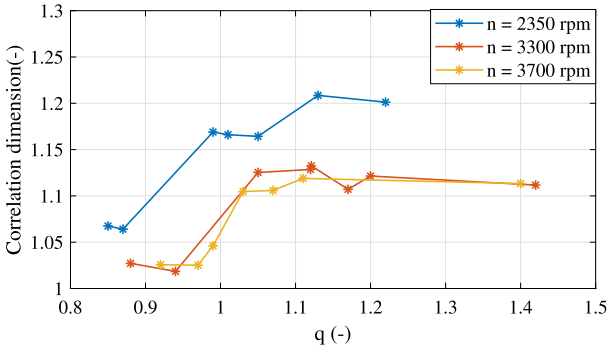

Fig. 15. Correlation dimension of the low-pass filtered pressure signal and different shaft speeds.

The presented results showed a relative decrease in the value of the correlation dimension whenever the operating point approached the area where the stall was imminent, with no audible manifestations or mechanical vibrations of the compressor present yet. The disadvantage of the analyses presented for real-time evaluation, necessary for implementation in the control system of the compressor station, is the necessity of data filtering and subsequent time-consuming processing. However, both mentioned disadvantages can be reduced. Lowpass filtering and subtraction of the DC component of the signal can be performed at the hardware level, thus in real time. The time-consuming analyses involved in evaluating d_{corr} are largely related to the determination of τ and m. In a real operation, however, these parameters do not need to be determined continuously. It is sufficient to determine the correct values after the machine is started and further evaluate the correlation dimension without the need for FNN and AMI algorithms.

The correlation dimension of the output pressure signal can be included among the monitored diagnostic parameters of the compressor station control system. A practical application may be based on the creation of a database of reference values d_{corr} for the desired range of machine working parameters. The control system can then compare the data collected online with the reference values, evaluate the risk of a stall and take action. In this case, however, a sufficiently large number of measurements on each of the monitored compressors need to be taken. The second option is to monitor only relative changes in d_{corr} without a previous reference where a decrease in the correlation dimension will indicate a risk of stall. However, the detection method will fail as long as the compressor flow rate is close to $q = 1$ immediately after starting up. The possibility of using the correlation dimension as one of the parameters in training a self-learning algorithm is also realistic. Here, training could take place on-the-fly, where the compressor station operators would manually identify compliant and non-compliant operating conditions, an activity already performed for long-term diagnostic purposes. In such an implementation, the results obtained by non-linear feature extraction would be correlated with a wide range of other diagnostic parameters, thus making stall protection more robust.

5. Conclusions

The experimental data were obtained by measurements on a scaled model of the first stage of the compressor integrated at the KS1 natural gas compressor station in Veľké Kapušany. The analysed signal (dynamic pressure waveform), taken just at the compressor outlet, was subjected to analysis in both the time and frequency domains. In the time domain, no significant change in signal was detected when the flow rate was reduced, even when vibrations and compressor noise were evident. However, in the frequency domain, an increase in amplitudes was observed at frequencies from 0 to 15 Hz, which appeared at $q \leq 1$, i.e. whenever the compressor reached a flow corresponding to the maxima of the performance curves or lower. Further signal processing consisted of phase-space reconstruction and qualitative and quantitative analysis of the resulting attractors. Assessing the qualitative change of the attractor did not yield new insights compared to FFT analysis. By using a quantifier of signal complexity (correlation dimension),

it was possible to detect changes in the dynamics of the measured signal when the compressor operating point approached the $q = 1$ threshold, that is, before the power curves were affected or vibration and noise were generated.

The analysis of quantitative attractor parameters as presented in the article can be incorporated into the compressor station control system as an additional monitored parameter. The advantage is that the signal is taken outside the compressor body without the need for modifications on the machine itself. Another advantage is the ability to recognise signs of compressor operation in mode when further reduction of the flow rate may mean the occurrence of vibrations, which will allow the control system to select a more suitable alternative for the connection of the individual machines to achieve the desired output flow of the compressor station. The disadvantages of the method are the necessity of filtering the measured signal and the relatively high computational power requirements for the evaluation of the monitored parameter (correlation dimension).

In general, phase-space reconstruction must be approached sensitively, as the choice of time lag and embedding dimension can greatly affect the results of the analyses. We have shown that the AMI and FNN algorithms are good guides in determining these parameters to indicate stall.

CRediT authorship contribution statement

Marek Mlkvik: Formal analysis, Writing – original draft, Writing – review & editing. **Robert Olšiak:** Investigation, Methodology. **Branislav Knížat:** Funding acquisition, Project administration, Resources.

Declaration of competing interest

The authors declare that they have no known competing financial interests or personal relationships that could have appeared to influence the work reported in this paper.

Data availability

The authors do not have permission to share data.

Acknowledgement

This article was written thanks to the generous support from the Operational Program Integrated Infrastructure for the project: “Research of physical, technical and material aspects of high-temperature reactors with the potential of hydrogen production”, project no. 313011BUH7, co-financed by the European Regional Development Fund. This work was also supported by the Slovak grant agency KEGA, project no. 016STU-4/2022.

Appendix A. List of measurement devices

quantity	sensor	range	accuracy
p_b	BD sensors DMP 331	90 – 110 kPa, abs.	0.5%
η	BD Sensorika HTP-6214	0-100%	1%
t_{amb}	BD Sensorika HTP-6214	0-40 °C	0,1%
p_{in}, p_{out}	SMI corp. SM-5312	206.85 kPa abs.	linearity ±0.5%
Δp_C	BD Sensors DPS200	0-10 kPa (diff)	1%
t_{in}, t_{out}	ZPA RTD		class A (0.15+0.002t)°C
Q (annubar)	dietrich standard 300/25		2%
Δp (annubar)	FSM DPS	0-500 Pa (diff)	1%
Torque	HBM T 30 FN	± 200 Nm	0.2%
n	HBM T 30 FN	± 6000 rpm	0.2%
p_{dyn}	PCB S112A22	± 345 kPa	linearity ≤ 1%
Q (nozzle)	ISA, $\beta = 0.5$		0.5%
Δp (nozzle)	BD Sensors DPS 330	0-10 kPa (diff)	1%

- annubar probe was calibrated by reference measurement by Prandtl tube in accordance with ANSI/AMCA standard 210-16)
- signal amplifiers with accuracy 0.1% were used when necessary. The effect of amplifiers was included in the calculations of measurement uncertainties.

References

[1] W.A. Benser, J.J. Moses, An investigation of backflow phenomenon in centrifugal compressors, Tech. Rep., National Advisory Committee for Aeronautics, 1945.
[2] W. Jansen, Rotating stall in a radial vaneless diffuser, ASME J. Basic Eng. 86 (1945) 750–758.
[3] T.R. Camp, I.J. Day, A study of spike and modal stall inception in a low-speed axial compressor, ASME J. Turbomach. 120 (1998).
[4] M. Inoue, M. Kuroumaru, T. Tanino, S. Yoshida, M. Furukawa, Comparative studies on short and long length-scale stall cell propagating in an axial compressor rotor, ASME J. Turbomach. 123 (2001) 24–30.

[5] G. Pullan, A. Young, I. Day, E. Greitzer, Z. Spakovszky, Origins and structure of spike-type rotating stall, ASME J. Turbomach. 137 (2015).
[6] I. Day, Stall, surge, and 75 years of research, ASME J. Turbomach. 138 (2016).
[7] H. Emmons, Compressor surge and stall propagation, Trans. Am. Soc. Mech. Eng. 77 (1955) 455–467.
[8] B. Gu, D. Xu, X. Dong, D. Sun, X. Sun, A modified small perturbation stability prediction model for axial compressors with circumferential inlet distortion, Aerosp. Sci. Technol. 132 (2023) 108079, https://doi.org/10.1016/j.ast.2022.108079, https://www.sciencedirect.com/science/article/pii/S1270963822007532.
[9] A. Stenning, Stall propagation in cascades of airfoils, ASME Trans. 80 (1958), https://doi.org/10.1115/1.4012510.
[10] J. Fabri, R. Siestrunck, Rotating stall in axial flow compressors, J. Aeronaut. Sci. 24 (1970), https://doi.org/10.1115/1.4012510.
[11] V.-M. Lei, Z.S. Spakovszky, E.M. Greitzer, A criterion for axial compressor hub-corner stall, J. Turbomach. 130 (3) (05 2008).
[12] B. Liu, D. Fu, X. Yu, Maximum Loading Capacity of Tandem Blades in Axial Compressors, Vol. Volume 2C: Turbomachinery of Turbo Expo: Power for Land, Sea, and Air, 2020.
[13] J. Li, L. Ji, An improved prediction model for corner stall in axial compressors with dihedral effect, Chin. J. Aeronaut. 33 (5) (2020) 1433–1443, https://doi.org/10.1016/j.cja.2019.12.031, https://www.sciencedirect.com/science/article/pii/S1000936120301096.
[14] H. Li, Q. Zheng, B. Jiang, Influence of rotor-stator axial clearance on compressor rotating stall characteristics, Aerosp. Sci. Technol. 139 (2023) 108373, https://doi.org/10.1016/j.ast.2023.108373, https://www.sciencedirect.com/science/article/pii/S1270963823002705.
[15] J. Wang, B. Wang, H. Yang, Z. Sun, K. Zhou, X. Zheng, Compressor geometric uncertainty quantification under conditions from near choke to near stall, Chin. J. Aeronaut. 36 (3) (2023) 16–29, https://doi.org/10.1016/j.cja.2022.10.012, https://www.sciencedirect.com/science/article/pii/S1000936122002527.
[16] C. Yang, L. Fu, C. Hu, X. Shi, Modelling and dynamic mode analysis of compressor impeller spike-type stall with global stability approach, Int. J. Mech. Sci. 201 (2021) 106486, https://doi.org/10.1016/j.ijmecsci.2021.106486, https://www.sciencedirect.com/science/article/pii/S0020740321002216.
[17] S. Moru, Y. Bo, W. Yueheng, Z. Rui, L. Zixuan, Analysis on spike-type rotating stall in transonic axial compressor by dynamic mode decomposition, Aerosp. Sci. Technol. 131 (2022) 108008, https://doi.org/10.1016/j.ast.2022.108008, https://www.sciencedirect.com/science/article/pii/S1270963822006824.
[18] X.-J. Yu, B.-J. Liu, Stereoscopic piv measurement of unsteady flows in an axial compressor stage, Exp. Therm. Fluid Sci. 31 (8) (2007) 1049–1060, https://doi.org/10.1016/j.expthermflusci.2006.11.001, https://www.sciencedirect.com/science/article/pii/S0894177706001804.
[19] X.-D. Liu, Y.-J. Li, Z.-Q. Liu, W. Yang, R. Tao, Dynamic evolution process of rotating stall vortex based on high-frequency piv system in centrifugal impeller, Ocean Eng. 259 (2022) 111944, https://doi.org/10.1016/j.oceaneng.2022.111944, https://www.sciencedirect.com/science/article/pii/S002980182201280X.
[20] B. Liu, X. Xu, X. Yu, G. An, Method for utilizing piv to investigate high curvature and acceleration boundary layer flows around the compressor blade leading edge, Chin. J. Aeronaut. 35 (12) (2022) 72–88, https://doi.org/10.1016/j.cja.2022.04.013, https://www.sciencedirect.com/science/article/pii/S1000936122000784.
[21] M.M. Bright, H.K. Qammar, H.J. Weigl, J.D. Paduano, Stall precursor identification in high-speed compressor stages using chaotic time series analysis methods, J. Turbomach. 119 (3) (1997) 491–499, https://doi.org/10.1115/1.2841148, https://asmedigitalcollection.asme.org/turbomachinery/article-pdf/119/3/491/5631736/491_1.pdf.
[22] I.J. Day, Stall inception in axial flow compressors, J. Turbomach. 115 (1) (1993) 1–9.
[23] M. Tryfonidis, O. Etchevers, J.D. Paduano, A.H. Epstein, G.J. Hendricks, Prestall behavior of several high-speed compressors, J. Turbomach. 117 (1) (1995) 62–80.
[24] L. Wang, J. Zhang, W. Zhang, Identify the rotating stall in centrifugal compressors by fractal dimension in reconstructed phase space, Entropy 17 (12) (2015) 7888–7899, https://doi.org/10.3390/e17127848, cited By 11.
[25] F. Lou, N.L. Key, Compressor stall warning using nonlinear feature extraction algorithms, J. Eng. Gas Turbines Power 142 (12) (11 2020) 121005, https://doi.org/10.1115/1.4048990, https://asmedigitalcollection.asme.org/gasturbinespower/article-pdf/142/12/121005/6595749/gtp_142_12_121005.pdf.
[26] X. Xue, T. Wang, Stall recognition for centrifugal compressors during speed transients, Appl. Therm. Eng. 153 (2019) 104–112, https://doi.org/10.1016/j.applthermaleng.2019.02.027.
[27] ASME, Performance Test Code on Compressors and Exhausters, ASME PTC 10-1997, 1998.
[28] ANSI, Laboratory Methods of Testing Fans for Certified Aerodynamic Performance Rating, An American National Standard Approved by ANSI, 2007.
[29] M. Casdagli, S. Eubank, D.J. Farmer, State space reconstruction in the presence of noise, Physica D 51 (1–3) (1991).
[30] J. Park, J. Cha, S. Lee, Experimental investigation on performance test of 150-kw-class supercritical co2 centrifugal compressor, Appl. Therm. Eng. 210 (2022), https://doi.org/10.1016/j.applthermaleng.2022.118310, cited By 1.
[31] S. Wallot, D. Monster, Calculation of Average Mutual Information (AMI) and False-Nearest Neighbors (FNN) for the estimation of embedding parameters of multidimensional time series in Matlab, Front. Psychol. 9 (8 2018).
[32] M.B. Kennel, R. Brown, H.D.I. Abarbanel, Determining embedding dimension for phase-space reconstruction using a geometrical construction, Phys. Rev. A 45 (1992) 3403–3411, https://doi.org/10.1103/PhysRevA.45.3403, https://link.aps.org/doi/10.1103/PhysRevA.45.3403.